

On the super-resolution capacity of imagers using unknown speckle illuminations

December 8, 2024 - Jérôme Idier, *Member, IEEE*, Simon Labouesse, Marc Allain, Penghuan Liu, Sébastien Bourguignon, and Anne Sentenac.

Abstract—Speckle based imaging consists in forming a super-resolved reconstruction of an unknown sample from low-resolution images obtained under random inhomogeneous illuminations (speckles). In a blind context where the illuminations are unknown, we study the *intrinsic* capacity to recover spatial frequencies beyond the cut-off frequency, without *a priori* assumption on the sample. We demonstrate that, under physically realistic conditions, the correlation of the data have a super-resolution power corresponding to the squaring of the imager point spread function. This theoretical result is important for many practical imaging systems such as acoustic and electromagnetic tomographies, fluorescence and photoacoustic microscopies, or synthetic aperture radar imaging. A numerical validation is proposed in the case of fluorescence microscopy.

Index Terms—Multi-illumination imaging, High-resolution, Cutoff frequency, Second-order statistics, Optical microscopy, Photoacoustic imaging, Synthetic aperture radar

I. INTRODUCTION

In most active wave imaging systems, the recorded data z can be modeled as the convolution with a point spread function (PSF) h of the product of the sample ρ with an illumination E , plus some additive noise ε :

$$z = h \star (\rho E) + \varepsilon \quad (1)$$

where \star stands for the convolution operator, either in two or three spatial dimensions. This simple model applies to imaging configurations as diverse as microwave scanners or anechoic chambers [1], radar remote sensing [2] or fluorescence microscopy [3].

The point spread function h contains the information on the imager geometry such as the numerical aperture (NA) of the microscope objective or the size of the antenna array in radar imaging. It accounts for the wave propagation from the sample to the detector. In most configurations, the free-space propagation prevents the wavefield high frequencies to reach the detector. As a result, h has necessarily a bounded Fourier support \mathcal{D}_{PSF} . For instance, in a microwave scanner, \mathcal{D}_{PSF} is a sphere of radius $1/\lambda$ (where λ is the illumination wavelength) when the field scattered by the sample is recorded under all

possible directions, or a cap of sphere when the observation is performed only over a small solid angle [4]. Similarly, in two (or three) dimensional fluorescence microscopy, \mathcal{D}_{PSF} is a disk (or a solid torus) of radius NA/λ [3].

When the illumination is homogeneous throughout the target, solely the sample frequency components in \mathcal{D}_{PSF} can be restored from the data, which limits fundamentally the image resolution. To improve the latter, synthetic imaging using multiple illuminations has been developed. Its main principle is to use several inhomogeneous illuminations $E_m, m = 1, \dots, M$, to probe the sample. The frequency mixing of E_m with ρ results in a down-modulation of the sample high spatial frequencies into the frequency-support \mathcal{D}_{PSF} of the point spread function. Using an appropriate data processing, sample frequencies beyond \mathcal{D}_{PSF} can be recovered, yielding a much better resolution. This idea is at the core of many imaging configurations such as Synthetic Aperture Radar (SAR) [2], diffraction tomography [5], and Structured Illumination fluorescence Microscopy (SIM) [6], [7], among others.

In all these imaging modalities, the standard numerical or analogical process that forms the super-resolved image from the stack of low resolution data requires the precise knowledge, and thus the tight control, of the different illuminations. The super-resolution capacity of the process is then both theoretically and practically demonstrated. However, the full control of the illumination patterns is a major constraint for the experimental implementation and in some cases proves impossible. Hence, some groups have developed reconstruction algorithms able to handle some imprecision on the illuminations [8]–[11]. Following a more radical option, others have advocated the use of totally uncontrolled illuminations of speckle type [12]. This recent blind approach, which simplifies dramatically the experimentation, has been already implemented in optical microscopy [13]–[16] and photoacoustic imaging [17]. Using inversion schemes taking advantage of information on the illumination statistics and/or on the sample itself, the stack of low resolution speckle data yielded reconstructed images with a significantly better resolution than that provided by a standard imager using homogeneous illumination [13]–[16]. However, many questions remain unanswered about the theoretical resolution that one can expect from such a system, in particular with respect to the speckle statistics.

To the best of our knowledge, this paper provides the first comprehensive mathematical understanding of the super-resolution (SR) capacity of synthetic imaging using speckle illuminations in a blind way. Our analysis is very general and

The authors also acknowledge partial financial support for this paper from the GdR 720 ISIS and the Agence Nationale de la Recherche (ANR-12-BS03-0006).

J. Idier, P. Liu and S. Bourguignon are with L'UNAM Université, Ecole Centrale Nantes and the CNRS at the Institut de Recherche en Communications and Cybernétique de Nantes (IRCCyN, CNRS UMR 6597), F-44321 Nantes, France. E-mail: firstname.name@ircyn.ec-nantes.fr.

S. Labouesse, M. Allain and A. Sentenac are with Aix Marseille Univ, CNRS, Centrale Marseille, Institut Fresnel, F-13013 Marseille, France. E-mail: firstname.name@fresnel.fr.

basically holds as soon as the data can be modeled by Eq. (1) with $\rho \geq 0$. In particular, it applies to microwave, acoustic or holography imaging, where the data, the illuminations and the PSF are complex-valued, provided that the sample is lossless dielectric. It also applies to fluorescence microscopy, where all spatial quantities take real (nonnegative) values. In what follows, we will consider the complex-valued setting, since the real-setting can be deduced straightforwardly as a particular case where the imaginary parts of the relevant quantities vanish.

We consider M images (z_1, \dots, z_M) of the same sample that have been acquired using M different speckle illuminations. Each image $z_m = (z_m(\mathbf{r}_1), \dots, z_m(\mathbf{r}_N))$ is a set of N pixels, each of which being indexed by a spatial coordinate vector \mathbf{r}_n . In practice, vector \mathbf{r}_n spans a finite d -dimensional rectangular grid \mathcal{G} , common to all images, d being equal to two or three. By convention, we consider here that z_m are column vectors (obtained by scanning the image grid in an arbitrary order). The observation model reads

$$z_m(\mathbf{r}) = y_m(\mathbf{r}) + \varepsilon_m(\mathbf{r}) \quad (2)$$

for all $m = 1 \dots M$ and $\mathbf{r} \in \mathcal{G}$, with

$$y_m(\mathbf{r}) = \int h(\mathbf{r} - \mathbf{r}') \rho(\mathbf{r}') E_m(\mathbf{r}') d\mathbf{r}', \quad (3)$$

where E_m and ε_m are random quantities: E_m is the m th speckle illumination and ε_m stands for electronic noise. If the measurement process relies on counting discrete particles (*e.g.*, photon counting in optical microscopy), assuming that $y_m(\mathbf{r})$ is a real quantity, the observation model (2) can be replaced by

$$z_m(\mathbf{r}) = p_m(\mathbf{r}) + \varepsilon_m(\mathbf{r}) \quad (4)$$

with $p_m(\mathbf{r})$ a Poisson random variable of mean $y_m(\mathbf{r})$. In this case, the Poisson outcomes are assumed jointly statistically independent. Furthermore, the following assumptions are considered with the observation model (2) and (4):

- (i) The PSF h is both integrable and square-integrable (*i.e.*, $\int |h(\mathbf{x})|^p d\mathbf{x} < \infty$ for $p = 1, 2$), and it is positive semi-definite (*i.e.*, its Fourier transform is real, nonnegative). Moreover, its Fourier transform takes finite values and vanishes outside a closed set $\mathcal{D}_{\text{PSF}} = \{\mathbf{u} \mid \tilde{h}(\mathbf{u}) > 0\}$. These assumptions are met as soon as the measurement z_m is obtained in the far-field domain which is the case of most imaging systems [4].
- (ii) The sample ρ takes finite, nonnegative values within a closed and bounded domain \mathcal{F} , and vanishes outside \mathcal{F} .
- (iii) The noise and illuminations are second-order stationary, mutually decorrelated random processes. This is a standard hypothesis which is verified for most imagers [12, Sec. 4.4]. Moreover, a direct extension would be possible to cases where the statistical mean of the illuminations is spatially varying. Without loss of generality, we will also assume that the noise is centered.
- (iv) The first two moments of the illuminations are known. This fundamental assumption is at the core of our approach. It is expected to be less difficult to satisfy than the knowledge of the illuminations themselves.

In this work, we restrict the analysis of the data by considering only second-order statistics, *i.e.*, the statistical mean and covariance of the data. More precisely, our aim is to determine the spatial frequency domain over which the sample spectrum can be identified from these statistics. Such a restriction is legitimate for several reasons.

On the one hand, the empirical mean and covariance are easily accessible statistical quantities, that can provide reliable second-order information from a practically acceptable number of illuminations.

On the other hand, the statistical mean and covariance are exhaustive statistics if the data are Gaussian, whether they are real-valued or complex circular. For instance, the latter assumption is suited to most coherent imaging techniques such as electromagnetic tomography, acoustic tomography, and radar imaging. In other situations, such as optical fluorescence microscopy, the speckle illumination, and hence the data, are non-Gaussian. The statistical mean and covariance do not summarize all the information about the sample available in the measurements in such situations, but our results still provide a *lower bound* on the information retrievable from the complete data statistics.

In order to characterize the SR potential of second-order methods, we wish to assign each component of the spatial Fourier transform $\tilde{\rho}(\mathbf{u})$ of the imaged sample (hereinafter, the tilde sign \sim denotes the spatial Fourier transform) to one of the three classes:

- *Non-identifiable* spectral components are those for which the second-order data statistics bring no information.
- *Partially identifiable* components are those for which the second-order data statistics bring some information, but for which some ambiguity remains.
- *Identifiable* components are those which are uniquely determined given the second-order data statistics.

Obviously, these domains may depend on the frequency support \mathcal{D}_{PSF} and on the correlation structure of the speckle illumination.

Section II introduces precise notations and establishes expressions for the first two moments of the observed images as functions of the sample of interest ρ . Sections III and IV examine the dependency between the latter expressions and the spatial frequency components of the sample, in the case of uncorrelated and correlated speckles, respectively. The main mathematical result is obtained in the latter case. It is stated as Property 5 and the proof can be found in Appendix B. Section V deals with the practical question of a computational scheme to reconstruct the unknown scene from the data empirical second-order statistics. A two-dimensional SIM case is considered, and numerical simulation results are provided. Finally, Section VI discusses the practical consequences of the obtained results, and evokes possible extensions and remaining points to address.

II. FIRST AND SECOND-ORDER STATISTICS OF THE DATA

For simplicity reasons, the discrete, finite character of the data grid \mathcal{G} will be neglected, which amounts to assuming that it can be made arbitrary large and tight enough to reach a

lossless regime. On the one hand, the PSF h being frequency-limited to the bounded support \mathcal{D}_{PSF} , Parzen's multidimensional extension of Shannon theorem ensures that the ideal sampling of functions y_m is possible [18]. The same holds for z_m , or at least for a filtered version of z_m , where the pure noise components outside \mathcal{D}_{PSF} are rejected. On the other hand, we deduce from assumptions (i) that h has a non limited support (since its Fourier transform is of limited support), but it vanishes at arbitrary large distance from the origin (since its Fourier transform \tilde{h} is integrable).

The statistical mean and correlation of the data are now derived. In what follows, $*$ denotes complex conjugacy. According to assumption (iii), let $\mathcal{E}\{E\} = E_0$ and $\gamma_E(\mathbf{r}) = \mathcal{E}\{E(\mathbf{x})E^*(\mathbf{x} - \mathbf{r})\} - |E_0|^2$ denote the mean and correlation function of the speckle, and let $\gamma_\varepsilon(\mathbf{r}) = \mathcal{E}\{\varepsilon(\mathbf{x})\varepsilon^*(\mathbf{x} - \mathbf{r})\}$ denote the correlation function of the noise.

A. First-order information content

From the observation model (2)-(3) and from the assumption of centered noise, we deduce the statistical mean $\mu_z(\mathbf{r}) = \mathcal{E}\{z_m(\mathbf{r})\}$:

$$\mu_z(\mathbf{r}) = \mathcal{E}\{y_m(\mathbf{r})\} = E_0 \int h(\mathbf{r} - \mathbf{r}')\rho(\mathbf{r}') d\mathbf{r}' \quad (5)$$

whose Fourier transform reads:

$$\tilde{\mu}_z(\mathbf{u}) = E_0 \tilde{h}(\mathbf{u}) \tilde{\rho}(\mathbf{u}). \quad (6)$$

If (2) is replaced by (4), Appendix A shows that (5) still holds.

A straightforward deduction from expression (6) is that any spectral component of ρ belonging to the support \mathcal{D}_{PSF} is identifiable, provided that $E_0 \neq 0$. In particular, if $E_m(\mathbf{r})$ is a complex circular Gaussian process, we get $E_0 = 0$ [12] and $\mu_z(\mathbf{r})$ brings no information about the unknown sample. This conclusion leads to the following property.

Property 1 *The frequency component $\tilde{\rho}(\mathbf{u})$ is identifiable from $\mu_z(\mathbf{r})$ if and only if $\mathbf{u} \in \mathcal{D}_1$ with*

$$\mathcal{D}_1 = \begin{cases} \mathcal{D}_{\text{PSF}} & \text{if } E_0 \neq 0, \\ \emptyset & \text{otherwise.} \end{cases}$$

In any case, the first-order does not convey any information on the spectral components outside \mathcal{D}_{PSF} , i.e., it brings no SR capacity.

B. Second-order information content

Now let us focus on the data correlation function

$$\gamma_z(\mathbf{r}, \mathbf{r}') = \mathcal{E}\{z_m(\mathbf{r})z_m^*(\mathbf{r}')\} - \mu_z(\mathbf{r})\mu_z^*(\mathbf{r}').$$

In the case where (2) holds, we immediately get

$$\gamma_z(\mathbf{r}, \mathbf{r}') = \gamma_y(\mathbf{r}, \mathbf{r}') + \gamma_\varepsilon(\mathbf{r} - \mathbf{r}'). \quad (7)$$

with:

$$\begin{aligned} \gamma_y(\mathbf{r}, \mathbf{r}') &= \mathcal{E}\{y_m(\mathbf{r})y_m^*(\mathbf{r}')\} - \mathcal{E}\{y_m(\mathbf{r})\}\mathcal{E}\{y_m^*(\mathbf{r}')\} \\ &= \iint \rho(\mathbf{x})\rho(\mathbf{x}') h(\mathbf{r} - \mathbf{x})h^*(\mathbf{r}' - \mathbf{x}') \gamma_E(\mathbf{x} - \mathbf{x}') d\mathbf{x} d\mathbf{x}'. \end{aligned} \quad (8)$$

from (3) and (5). In the case where (4) holds, Appendix A shows that (7) contains an additional term $\mu_z(\mathbf{r})\delta_K(\mathbf{r} - \mathbf{r}')$ where δ_K stands for the Kronecker function, i.e., $\delta_K(\mathbf{r}) = 1$ if $\mathbf{r} = \mathbf{0}$ and zero otherwise.

Remark 1 *In the Poisson noise case, the additional term $\mu_z(\mathbf{r})$ is proportional to E_0 , whereas $\gamma_y(\mathbf{r}, \mathbf{r}')$ varies as $\gamma_E(\mathbf{r}, \mathbf{r}')$, which is proportional to E_0^2 in optics [12]. Therefore, accounting for the Poisson statistics of the data in optics may be useful in the low intensity case only.*

In all cases, the only potential source of information about the spectral components outside \mathcal{D}_{PSF} is the term $\gamma_y(\mathbf{r}, \mathbf{r}')$ that we now examine in a deeper way. Using a double Fourier transform on (8), we obtain

$$\begin{aligned} \tilde{\gamma}_y(\mathbf{u}, \mathbf{u}') &= \tilde{h}(\mathbf{u})\tilde{h}(-\mathbf{u}') \\ &\iint e^{-2i\pi(\mathbf{u}\cdot\mathbf{x} + \mathbf{u}'\cdot\mathbf{x}')} \rho(\mathbf{x})\rho(\mathbf{x}') \gamma_E(\mathbf{x} - \mathbf{x}') d\mathbf{x} d\mathbf{x}' \end{aligned} \quad (9)$$

where $\mathbf{u} \cdot \mathbf{x}$ denotes the usual scalar product in \mathbb{R}^d . Given that

$$\gamma_E(\mathbf{x}' - \mathbf{x}) = \int e^{2i\pi(\mathbf{x} - \mathbf{x}') \cdot \mathbf{u}''} \tilde{\gamma}_E(\mathbf{u}'') d\mathbf{u}'',$$

it is easy to express $\tilde{\gamma}_y(\mathbf{u}, \mathbf{u}')$ as follows:

$$\tilde{\gamma}_y(\mathbf{u}, \mathbf{u}') = \tilde{h}(\mathbf{u})\tilde{h}(-\mathbf{u}') \tilde{g}(\mathbf{u}, \mathbf{u}'), \quad (10)$$

with

$$\tilde{g}(\mathbf{u}, \mathbf{u}') = \int \tilde{\rho}(\mathbf{u} - \mathbf{u}'') \tilde{\rho}(\mathbf{u}' + \mathbf{u}'') \tilde{\gamma}_E(\mathbf{u}'') d\mathbf{u}''. \quad (11)$$

According to expressions (8) or (10)-(11), the spectral density $\tilde{\gamma}_E$ clearly plays a central role in the identification of the spectral components of the sample. However, a difficulty to analyse the SR capacity of second-order methods comes from the fact that the data correlation is not a linear but rather a quadratic functional of the unknown sample ρ . As a consequence, no general theory can be applied to solve equations (8) or (10)-(11) for ρ . In the following two sections, we investigate two important cases, namely the case of spatially uncorrelated speckle, and the case of correlated speckle with a frequency support contained in the frequency support of the PSF. In both cases, it turns out possible to predict some SR results.

III. CASE OF UNCORRELATED SPECKLE

Let us assume that $\gamma_E(\mathbf{r}) = \gamma_E(\mathbf{0})\delta(\mathbf{r})$, where δ is a Dirac distribution. This assumption can be considered valid when the speckle correlation typical size is much smaller than that of the point spread function. Then (8) becomes

$$\gamma_y(\mathbf{r}, \mathbf{r}') = \gamma_E(\mathbf{0}) \int \rho^2(\mathbf{x}) h(\mathbf{r} - \mathbf{x})h^*(\mathbf{r}' - \mathbf{x}) d\mathbf{x}. \quad (12)$$

In the Fourier domain, $\tilde{\gamma}_E(\mathbf{u}) = \gamma_E(\mathbf{0})$, so (11) and (10) read

$$\begin{aligned} \tilde{g}(\mathbf{u}, \mathbf{u}') &= \gamma_E(\mathbf{0})\rho^2(\mathbf{u} + \mathbf{u}'), \\ \tilde{\gamma}_y(\mathbf{u}, \mathbf{u}') &= \gamma_E(\mathbf{0})\tilde{h}(\mathbf{u})\tilde{h}(-\mathbf{u}') \rho^2(\mathbf{u} + \mathbf{u}'), \end{aligned} \quad (13)$$

respectively. The latter relation is important since it yields that ρ^2 is accessible over all frequencies $\mathbf{u} + \mathbf{u}'$ such that both \mathbf{u}

and $-\mathbf{u}'$ belong to \mathcal{D}_{PSF} , i.e., over the set $\mathcal{D}_{\text{PSF}} \ominus \mathcal{D}_{\text{PSF}}$, where \ominus denotes the Minkowski difference between sets:

$$A \ominus B = \{\mathbf{x} - \mathbf{y}, \mathbf{x} \in A, \mathbf{y} \in B\}$$

As a conclusion, the following property holds.

Property 2 *The frequency component $\tilde{\rho}^2(\mathbf{u})$ is identifiable from the correlation function $\gamma_y(\mathbf{r}, \mathbf{r}')$ if and only if $\mathbf{u} \in \mathcal{D}_2 = \mathcal{D}_{\text{PSF}} \ominus \mathcal{D}_{\text{PSF}}$.*

Remark 2 *A useful characterization of \mathcal{D}_2 is*

$$\mathcal{D}_2 = \{\mathbf{u} \mid \gamma_{\tilde{h}}(\mathbf{u}) > 0\} \quad (14)$$

where $\gamma_{\tilde{h}}$ is the (deterministic) autocorrelation function of \tilde{h} . Hence, if \tilde{h} is a disk of radius ν_{PSF} (e.g., \tilde{h} is the two-dimensional optical transfer function in fluorescence microscopy), we get $\mathcal{D}_1 \subset \mathcal{D}_2$ with \mathcal{D}_2 a disk of radius $2\nu_{\text{PSF}}$, so the SR factor on ρ^2 equals two.

A remarkable fact is that Property 2 still holds if only the variance $v(\mathbf{r}) = \gamma_y(\mathbf{r}, \mathbf{r})$ is considered instead of the full correlation function $\gamma_y(\mathbf{r}, \mathbf{r}')$. The starting point is the following identity, which is a direct consequence of (12):

$$v(\mathbf{r}) = \gamma_E(\mathbf{0}) (\rho^2 \star |h|^2)(\mathbf{r}), \quad (15)$$

i.e., in the Fourier domain:

$$\int v(\mathbf{r}) e^{-2i\pi\mathbf{r}\cdot\mathbf{u}} d\mathbf{r} = \gamma_E(\mathbf{0}) (\tilde{\rho}^2 \times \gamma_{\tilde{h}})(\mathbf{u}),$$

so the conclusion is immediate given (14).

Property 3 *The frequency component $\tilde{\rho}^2(\mathbf{u})$ is identifiable from the variance function $\gamma_y(\mathbf{r}, \mathbf{r})$ if and only if $\mathbf{u} \in \mathcal{D}_2$.*

We note that a similar statement was indeed made in [15] for a simplified imaging configuration made of fluorescent point-like samples.

Remark 3 *We have $\tilde{\rho}^2 = \tilde{\rho} \star \tilde{\rho}$, so the fact that $\tilde{\rho}^2$ can be retrieved on \mathcal{D}_2 does not imply that $\tilde{\rho}$ can be retrieved on the same domain, nor in any other domain. A simple counter-example is as follows (it is one-dimensional, but a multi-dimensional version can be easily devised): let us define a modulated sinc signal as*

$$\delta\rho(r) = \frac{\sin \pi r}{\pi r} \cos 2\pi\nu r,$$

where ν is a frequency parameter. Its Fourier transform is

$$\tilde{\delta\rho}(u) = \frac{1}{2}\text{rect}(u + \nu) + \frac{1}{2}\text{rect}(u - \nu),$$

where rect equals one within $[-1/2, 1/2]$ and zero elsewhere. Let us choose ν large enough so that the support of $\tilde{\delta\rho}$ does not intersect \mathcal{D}_2 (which is always possible since \mathcal{D}_2 is a frequency set of bounded support). Now let $\rho_1(r) = 1$ for all r and $\rho_2 = (1 + \delta\rho)^{1/2}$. We have that ρ_1^2 and ρ_2^2 identify within \mathcal{D}_2 , whereas $\tilde{\rho}_1$ and $\tilde{\rho}_2$ differ, even inside \mathcal{D}_2 . The latter fact can be checked by expressing $\tilde{\rho}_2$ using the Maclaurin series expansion of $(1 + \delta\rho)^{1/2}$.

IV. CASE OF CORRELATED SPECKLE

Let us now assume that the unknown speckle illuminations are spatially correlated, with a frequency support restricted to a frequency domain $\mathcal{D}_{\text{spec}}$. According to expression (10), $\tilde{\gamma}_y(\mathbf{u}, \mathbf{u}')$ vanishes when either \mathbf{u} or $-\mathbf{u}'$ is outside \mathcal{D}_{PSF} . On the other hand, according to (11), $\tilde{g}(\mathbf{u}, \mathbf{u}')$ conveys no information on the frequency components $\tilde{\rho}(\mathbf{v})$ such that either $\mathbf{v} \pm \mathbf{u}$ or $\mathbf{v} \pm \mathbf{u}'$ falls outside $\mathcal{D}_{\text{spec}}$. We conclude that the following property holds.

Property 4 *Any spectral component $\tilde{\rho}(\mathbf{u})$ such that $\mathbf{u} \notin \mathcal{D}_1 \cup \mathcal{D}_2'$ with $\mathcal{D}_2' = \mathcal{D}_{\text{PSF}} \ominus \mathcal{D}_{\text{spec}}$ is non-identifiable from the mean $\mu_z(\mathbf{r})$ and the correlation function $\gamma_y(\mathbf{r}, \mathbf{r}')$.*

Remark 4 *If each speckle pattern was known, the set of identifiable frequency components would be \mathcal{D}_2' , and the components outside \mathcal{D}_2' would remain non-identifiable. This case can be easily analyzed since it falls into the usual situation of controlled illumination patterns. In the same way, if the complete data statistics were available (the speckle patterns being unknown), the components outside \mathcal{D}_2' would also be non-identifiable, since the latter situation is not more favorable than the former. We thus conclude that frequency components outside \mathcal{D}_2' cannot be retrieved from standard (i.e., non Bayesian) statistical information, including higher moments.*

Property 4 is of negative nature. Fortunately, a positive partial converse can be established in the important situation where the frequency support of the illuminations is not larger than that of the PSF. The following non trivial property holds. Its proof is reported in Appendix B.

Property 5 *Provided that γ_E is such that $\mathcal{D}_{\text{spec}} \subseteq \mathcal{D}_{\text{PSF}}$, any spectral component $\tilde{\rho}(\mathbf{u})$ is identifiable from the mean $\mu_z(\mathbf{r})$ and the correlation function $\gamma_y(\mathbf{r}, \mathbf{r}')$ if $\mathbf{u} \in \mathcal{D}_1 \cup \mathcal{D}_2''$ with $\mathcal{D}_2'' = \mathcal{D}_{\text{spec}} \ominus \mathcal{D}_{\text{spec}}$.*

Remark 5 *Proposition 5 deals with the identifiability of the frequency components of the sample, but it does not predict the reachable estimation precision in the realistic situation of a limited set of noisy data.*

In the case where \mathcal{D}_{PSF} and $\mathcal{D}_{\text{spec}}$ are centered disks of respective radii ν_{PSF} and ν_{spec} (as in two-dimensional fluorescence microscopy), \mathcal{D}_2'' is a centered disk of radius $2\nu_{\text{spec}}$. As a consequence, if $E_0 \neq 0$, we get $\mathcal{D}_1 \subset \mathcal{D}_2''$ if $\nu_{\text{spec}} > \nu_{\text{PSF}}/2$, leading to a SR factor of $2\nu_{\text{spec}}/\nu_{\text{PSF}}$. Figure 1 is a graphical illustration for both Properties 4 and 5. Let us remark that the status of the frequency components outside the colored areas remains an open question. Our conjecture is that they are only partially identifiable from the second-order data statistics.

In the extreme case where $\mathcal{D}_{\text{spec}} = \mathcal{D}_{\text{PSF}}$, which is often encountered if the illuminations and observations are performed via the same components (same antenna array for the emission and detection, same microscope objective for the illumination and collection), the latter two properties allow

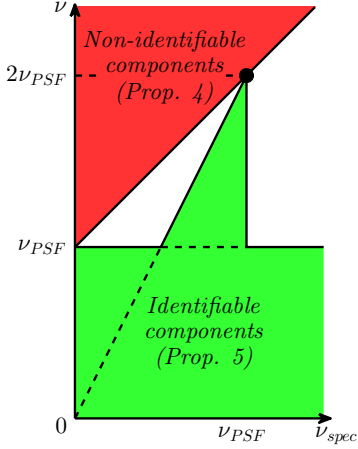


Fig. 1. Illustration of Props. 4 and 5 when \mathcal{D}_{PSF} and $\mathcal{D}_{\text{spec}}$ are centered disks of respective radii ν_{PSF} and ν_{spec} (and $E_0 \neq 0$). The cutoff frequency ν_{PSF} is fixed, while the speckle maximal frequency ν_{spec} varies along the X-axis. The range of identifiable and of non-identifiable frequency components are represented along the Y-axis.

us to reach a tight conclusion: second-order data statistics are sufficient to identify all the frequency components of the sample within $\mathcal{D}_2' \equiv \mathcal{D}_2' \equiv \mathcal{D}_2 = \mathcal{D}_{\text{PSF}} \ominus \mathcal{D}_{\text{PSF}}$, and bring no information outside (such a situation corresponds to the black dot on Fig. 1). In other words, they should permit to recover the sample with a resolution equivalent to that of $|h|^2$, akin to classical SIM in fluorescence microscopy.

The next section proposes a numerical speckle SIM example to illustrate that high frequency components within $\mathcal{D}_{\text{PSF}} \ominus \mathcal{D}_{\text{PSF}}$ can be reliably retrieved, with a SR capacity comparable to that of classical SIM.

V. NUMERICAL IMPLEMENTATION FOR 2D SPECKLE SIM

The goal of the present section is to give a practical illustration of Property 5, which is the main theoretical result of Section IV. For this purpose, we consider an idealized two-dimensional (2D) speckle illumination fluorescence microscopy problem. In the standard assumption of a perfect circular lens, h is the so-called Airy pattern [19, Sec. 4.4.2], and the optical transfer function (OTF) \tilde{h} defines a support $\mathcal{D}_{\text{PSF}} = \{\mathbf{u}, \|\mathbf{u}\|_2 < 2\text{NA}/\lambda\}$ with NA the numerical aperture of the microscope and λ the emission/excitation wavelength. We further assume that the illumination of the sample and the collection of the emitted light is performed through the same optical device. Ignoring the Stokes-shift¹, we consider hereafter that $\gamma_E = E_0^2 h$. According to Property 5, an SR effect approaching a factor two is expected from the empirical second-order statistics of a set of M collected images, for asymptotically large values of M . The goal here is to show empirically that this SR effect does happen in realistic conditions, and in particular for moderately large values of M .

¹The Stokes-shift [20] implies that the support \tilde{h} is slightly smaller than the support of $\tilde{\gamma}_E$. This difference between supports is small (about 10%) and we expect that it will have a negligible impact on the SR effect that should reach twice the cutoff frequency of the OTF.

A. Discretized model for 2D speckle SIM

For the sake of computer implementation, (3) must be replaced by its discretized counterpart

$$\mathbf{z}_m = \mathbf{H}\mathbf{R}\mathbf{E}_m + \boldsymbol{\varepsilon}_m, \quad (16)$$

where \mathbf{H} is a symmetric convolution matrix, and $\mathbf{R} = \text{Diag}(\boldsymbol{\rho})$, so that $\mathbf{R}\mathbf{E}_m$ corresponds to the product between the vectorized sample $\boldsymbol{\rho}$, and the vectorized m th illumination pattern \mathbf{E}_m . The mean vector and the covariance matrix of the acquisition \mathbf{z}_m now read

$$\boldsymbol{\mu}_z = E_0 \mathbf{H} \boldsymbol{\rho}, \quad \boldsymbol{\Gamma}_z = \mathbf{H} \mathbf{R} \boldsymbol{\Gamma}_E \mathbf{R} \mathbf{H} + \boldsymbol{\Gamma}_\varepsilon, \quad (17)$$

where $\boldsymbol{\Gamma}_E$ and $\boldsymbol{\Gamma}_\varepsilon$ are the covariance matrix of the speckle patterns and of the additive noise, respectively. For any finite number of illuminations M , the empirical mean $\hat{\boldsymbol{\mu}}_z$ and covariance $\hat{\boldsymbol{\Gamma}}_z$ are defined as

$$\hat{\boldsymbol{\mu}}_z = \frac{1}{M} \sum_{m=1}^M \mathbf{z}_m, \quad \hat{\boldsymbol{\Gamma}}_z = \frac{1}{M} \sum_{m=1}^M \mathbf{z}_m \mathbf{z}_m^\dagger - \hat{\boldsymbol{\mu}}_z \hat{\boldsymbol{\mu}}_z^\dagger, \quad (18)$$

where the symbol † stands for the transpose conjugate operator. As M grows, $\hat{\boldsymbol{\mu}}_z$ and $\hat{\boldsymbol{\Gamma}}_z$ respectively converge toward $\boldsymbol{\mu}_z$ and $\boldsymbol{\Gamma}_z$, so that spatial frequency components of the sample within \mathcal{D}_2' become identifiable, according to Prop. 5. With a view to propose a computationally effective strategy to retrieve the latter components, we first directly formulate the main elements of Prop. 5 and of its proof in a finite dimensional (*i.e.*, discretized) framework.

B. Matrix transposition of Property 5

In the discrete framework of model (16), the matrix formulation of Property 5 mostly relies on the one-to-one mapping between the asymptotically available covariance $\boldsymbol{\Gamma}_y = \mathbf{H} \mathbf{R} \boldsymbol{\Gamma}_E \mathbf{R} \mathbf{H}$ and the matrix $\mathbf{S} = \boldsymbol{\Gamma}_E^{1/2} \mathbf{R} \boldsymbol{\Gamma}_E^{1/2}$, provided that $\text{Ker } \mathbf{H} \subseteq \text{Ker } \boldsymbol{\Gamma}_E$ ($\text{Ker } \mathbf{M}$ denotes the set of vectors \mathbf{v} such that $\mathbf{M}\mathbf{v}$ is the null vector). When the latter condition holds, we can show that \mathbf{S} is the unique Hermitian positive semi-definite² square-root of

$$\mathbf{F} = \boldsymbol{\Gamma}_E^{1/2} \mathbf{H}^+ \boldsymbol{\Gamma}_y \mathbf{H}^+ \boldsymbol{\Gamma}_E^{1/2},$$

where $^+$ denotes the generalized inverse [21, Chap. 5]. Indeed, matrices \mathbf{F} and \mathbf{S} respectively correspond to kernels F and f introduced in the proof of Property 5 (see Appendix B). Whereas $\boldsymbol{\Gamma}_y$ quadratically depends on $\boldsymbol{\rho}$, \mathbf{S} exhibits a linear dependency with respect to $\boldsymbol{\rho}$, paving the way to an identifiability analysis *via* a standard eigenvalue decomposition.

C. Numerical estimation strategy

The reconstruction principle from the second-order data statistics amounts to finding $\boldsymbol{\rho}$ that makes the mean vector $\boldsymbol{\mu}_z$ and the covariance matrix $\boldsymbol{\Gamma}_z$ in (17) best match with the empirical quantities $\hat{\boldsymbol{\mu}}_z$ and $\hat{\boldsymbol{\Gamma}}_z$ defined by (18). Given the previous subsection, a simple idea to recover the identifiable

²A Hermitian matrix is positive semi-definite if and only if all of its eigenvalues are nonnegative.

components of $\tilde{\rho}$ would be to compute an approximation \hat{F} of matrix F from the empirical data statistics:

$$\hat{F} = \Gamma_E^{1/2} \mathbf{H}^+ \hat{\Gamma}_y \mathbf{H} \Gamma_E^{1/2},$$

where $\hat{\Gamma}_y = \hat{\Gamma}_z - \Gamma_\varepsilon$, with a view to extract a positive semi-definite square-root matrix \hat{S} . However, neither $\hat{\Gamma}_y$ nor \hat{F} are guaranteed to be positive semi-definite, so the existence of \hat{S} is not granted.

A preferable procedure consists in introducing an appropriate dissimilarity measure between the empirical and the theoretical second-order statistics of the data, and to minimize the dissimilarity to obtain an estimated sample $\hat{\rho}$. One possible choice of dissimilarity measure is the Kullback-Leibler divergence (KLD) $D(\rho) = D_{\text{KL}}(\mathcal{N}(\hat{\mu}_z, \hat{\Gamma}_z) \parallel \mathcal{N}(\mu_z, \Gamma_z))$, where $\mathcal{N}(\mu, \Gamma)$ is the normal distribution of mean μ and covariance Γ . According to [22, § 9.1], an explicit expression of $D(\rho)$ is:

$$D(\rho) = \frac{1}{2} \text{Tr}(\Gamma_z^{-1} \hat{\Gamma}_z) + (\mu_z - \hat{\mu}_z)^t \frac{\Gamma_z^{-1}}{2} (\mu_z - \hat{\mu}_z) + \frac{1}{2} \log \frac{|\Gamma_z|}{|\hat{\Gamma}_z|} - \frac{N}{2} \quad (19)$$

where $|\cdot|$ and $\text{Tr}(\cdot)$ are the determinant and the trace of a square matrix, respectively. Let us mention that D is proportional to the log-likelihood of the data under the assumption that the latter follow the normal distribution $\mathcal{N}(\mu_z, \Gamma_z)$ [23]. However, the minimizer of D is an unregularized solution, which is unstable with respect to the random fluctuations in the dataset. Therefore, a penalization term must be added to D . In the sequel, we choose a quadratic penalization term to stabilize the solution, so that the SR effect remains purely driven by the data term. The criterion to minimize is then

$$J(\rho) = D(\rho) + \frac{\beta}{2} \|\rho\|_2^2, \quad (20)$$

with $\beta \geq 0$ and $\|\cdot\|_2$ is the usual Euclidian norm. From a computational perspective, a closed-form minimizer cannot be found, so the minimization problem must be solved iteratively. Indeed, it is a so-called *structured covariance* type problem, for which the Expectation-Maximization (EM) algorithm can be implemented [23]–[25]. However, our tests indicate that the EM algorithm converges very slowly in the speckle SIM context. For this reason, we rather rely on a nonlinear conjugate gradient method, which turns out to produce more efficient iterations. It relies on the expression of the gradient of the penalized KLD (20) with respect to ρ (see Appendix C for a derivation):

$$\nabla J(\rho) = -([\Omega^t(\Delta_\Gamma + \delta_\mu \delta_\mu^t) \Omega] \circ \Gamma_E) \rho - E_0 \Omega^t \delta_\mu + \beta \rho, \quad (21)$$

displayed as a column vector, with $\Omega = \Gamma_z^{-1} \mathbf{H}$, $\delta_\mu = \hat{\mu}_z - \mu_z$, $\Delta_\Gamma = \hat{\Gamma}_z - \Gamma_z$, and \circ stands for the Hadamard (component-wise) product. Let us stress that each computation of the gradient needs the construction and the inversion of an $N \times N$ matrix (for an N -pixel size problem), which represents a prohibitive computing cost for realistic imaging problems. The design of less costly iterations for large-size problems is out of the scope of the present paper, but we are currently working on this crucial issue.

D. Numerical illustration for 2D speckle SIM

Numerical simulations are now considered to support that a significant SR effect can be obtained in speckle fluorescence SIM, even with a moderately large number of illumination patterns E_m . The ground truth ρ^* consists in the 2D 'star-like' fluorescence pattern depicted in Fig. 2(a). The convolution matrix \mathbf{H} modeling the microscope is built from the discretized OTF associated with a circular aperture [19, Eq. (6-32)]; the numerical aperture NA is set to 1.49 and the emission/excitation wavelength λ is arbitrary set to 1. For this configuration, the resolution limit of standard wide-field imaging is clearly visible in Fig. 2(c). According to (16), a set of $M \in \{100, 1000\}$ speckle patterns are simulated to produce M low-resolution microscope images $\{z_m\}_{m=1}^M$. The covariance matrix Γ_E is set to $E_0^2 \mathbf{H}$ (we assume $\gamma_E = E_0^2 h$) and each acquisition z_m is corrupted with an independent and identically distributed Gaussian noise such that the signal-to-noise ratio in each frame is set to 21.1 dB. From the dataset $\{z_m\}_{m=1}^M$, the statistics $\hat{\mu}_z$ and $\hat{\Gamma}_z$ (18) are built. The case of an infinite illumination number ($M = \infty$) is also addressed by considering the expected (*i.e.*, asymptotical) statistics $\hat{\mu}_z = \mu_z^*$ and $\hat{\Gamma}_z = \Gamma_z^*$, where μ_z^* and Γ_z^* are obtained from (17) by setting $\rho = \rho^*$. In all cases, we proceed to the iterative minimization of the penalized KLD (20) to estimate the sample, using the deconvolved wide-field image of Fig. 2(c) as an initial point. For the (noise-free) asymptotic statistics, the regularization parameter is set to $\beta = 0$ and, as expected, the reconstruction exhibits the doubled resolution predicted by Prop. 5, see Fig. 2(f) compared to Fig. 2(b,c). With 100 and 1000 illuminations, the SR factor is lower, but the reconstructions shown on Figs. 2(d,e) are still much more resolved than the wide-field image of Fig. 2(c). Moreover, the SR factor progressively grows with the illumination number M , the result at $M = 1000$ being close to the asymptotic regime.

VI. CONCLUSION AND PERSPECTIVES

We have mathematically demonstrated that the mean and the correlation function of low resolution images obtained with unknown, random illuminations permit to recover a super-resolved image of the sample, provided the first two statistical moments of the illuminations are fully characterized. Since this condition is expected to be less stringent to meet than the knowledge of each illumination, we believe that this result can be interesting in many practical situations.

In photoacoustic imaging using speckle illuminations, the autocorrelation of the random optical intensity can drop to a few hundreds of nanometers while the acoustic PSF h has a typical width of tens of microns. Hence, from the acoustic point of view, the illumination can be seen as an uncorrelated random process [17], [26], which is the case studied in Section III. Using optical speckle in a photoacoustic experiment would allow to retrieve the square of the optical absorption density with a resolution corresponding to an ameliorated PSF $h_{\text{ext}} = |h|^2$.

In fluorescence microscopy, if the speckle is generated through the same objective as the one used to collect the

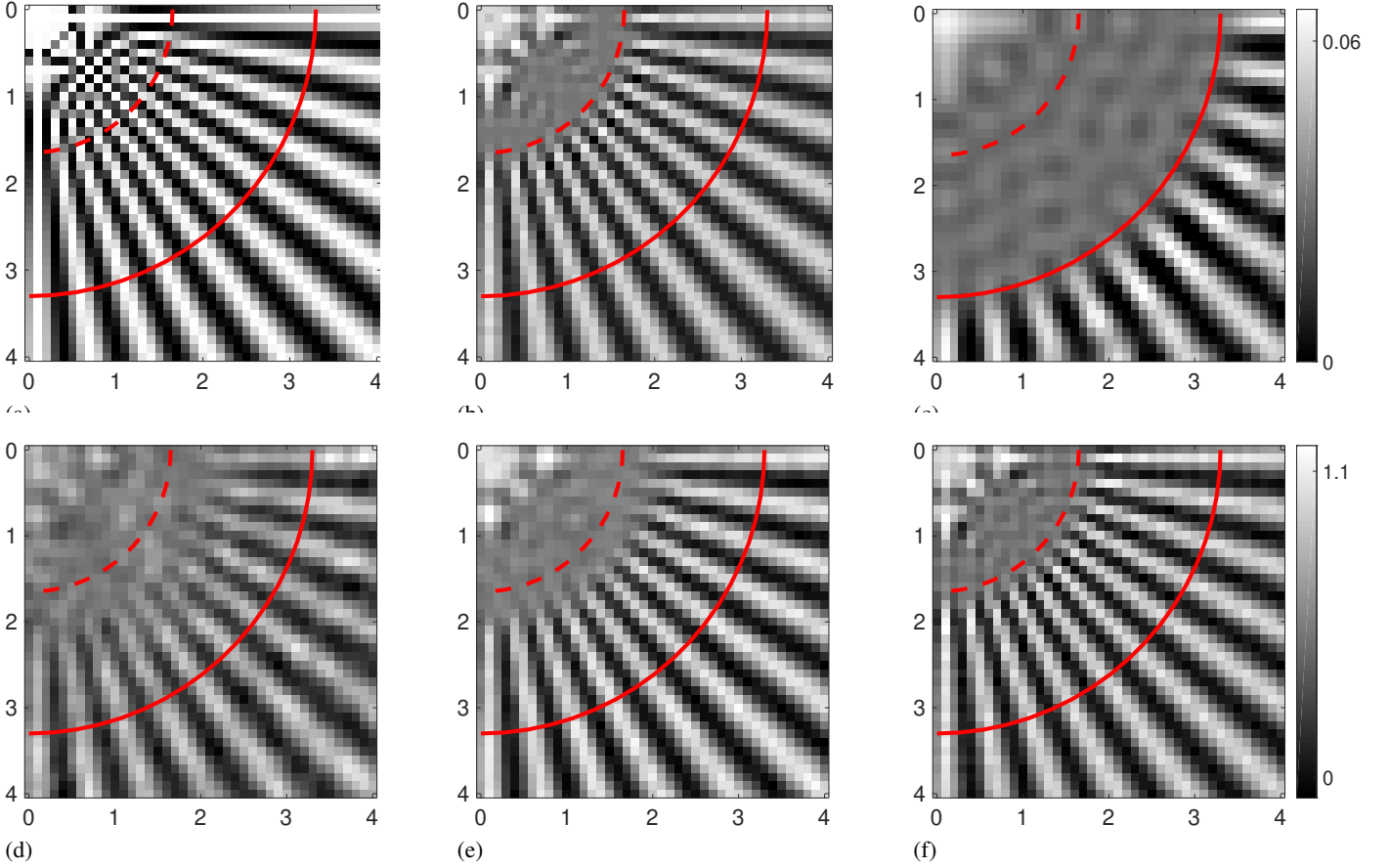


Fig. 2. (a) Lower quarter of the (80×80 pixels) ground-truth fluorescence pattern considered in [13]. (b) Filtered ground-truth retaining only the spatial frequency lower than twice the OTF limit. (c) Deconvolution of the wide-field (constant illumination) microscope acquisition. (d,e) Estimator of ρ obtained from the minimization of the penalized KLD (20) with $M = 100$ (d) and $M = 1000$ (e) speckle patterns; the regularization parameter is set to $\beta = \beta_0/M$ with $\beta_0 = 100$. (f) Estimator of ρ obtained from the minimization the KLD (19) with the asymptotic statistics $\hat{\mu} = \mu^*$ and $\hat{\Gamma} = \Gamma^*$. The distance units along the horizontal and vertical axes are given in wavelength λ . The image sampling step for all simulations is set to $\lambda/20$. The solid (resp. dashed) line corresponds to the spatial frequencies transmitted by the OTF support (resp. twice the OTF limit).

light, its autocorrelation is almost identical to the microscope PSF and Proposition 5 is also expected to apply. We believe that this is a particularly important result. Indeed, it shows that speckle microscopy has the potential to generate a super-resolved image corresponding to the PSF $h_{\text{ext}} = |h|^2$. In other words, the SR would be equivalent to that of a perfect confocal microscope with infinitively small pinhole [27], but it would be obtained with no transverse scanning and with no loss of photons.

In holographic imaging, the consequence could be even more spectacular. In holographic systems, the Fourier support of the PSF h is generally a cap of sphere. As a result, the three-dimensional information on the sample is lost if only one illumination is used. This is clearly observed in digital holography where the reconstruction of a target from its unique 2D hologram obtained under a monochromatic plane wave illumination is significantly deteriorated along one axis [28]. On the other hand, by processing 2D images obtained under different speckle illuminations, one should be able to reconstruct the target in three dimensions with a PSF comparable to that obtained in tomographic diffraction imaging [4], but without the difficulty and slowness of controlling the angles of illuminations.

Finally, it is important to stress the limits of the present analysis. First, the case of complex-valued samples (*i.e.*, with both dielectric and absorptive components) remains to be investigated, since it could have important implications in electromagnetic tomography. The present study can be easily adapted to the case of pure absorptive (imaginary) samples, but an extension to the more general case is not so direct. Second, our theoretical results are of asymptotic nature, in that they only predict the SR capacity of the imagers with an arbitrarily large number of illuminations. In particular, Proposition 5 does not provide the *sensitivity* of the retrievable sample frequency components. The simulation results shown in Section V-D nonetheless suggest that these frequency components can be retrieved with only a few hundreds of illuminations. Third, our results do not take into account the potential impact of advanced regularization in the inversion schemes (for instance, exploiting a sparsity prior [14] could yield an additional increase of resolution). Fourth, there exist many imaging configurations where the second-order statistics do not entirely characterize the probability distribution of the data (*e.g.*, when the speckle illuminations are positive intensities). In such cases, accounting more precisely for the speckle statistics could still ameliorate the resolution. According to Remark 4,

it is not the case when the support of the speckle correlation identifies with that of the PSF, but the question remains open in other cases. For instance, for uncorrelated speckles, one can write the following extension of Eq. (15),

$$\text{Cum}_y^n(\mathbf{r}, \dots, \mathbf{r}) = \text{Cum}_E^n(\mathbf{0}, \dots, \mathbf{0}) (\rho^n \star |h|^n)(\mathbf{r}), \quad (22)$$

where Cum^n denotes the n th circular cumulant of a given random process [29]. Equation (22) indicates that data higher-order statistics yield additional information on higher spatial frequencies of the sample. Such a property is reminiscent of the principle of SOFI [30].

The computational issue also remains broadly open, both in terms of memory requirements (to store the empirical data covariance matrix) and of computing time. The iterative scheme proposed in Subsection V-D is clearly limited to small-sized images. A challenge will be to accelerate the reconstruction process while preserving the SR capacity of speckle-based imaging, as characterized in this paper.

APPENDIX A CASE OF POISSON DATA

In the case where (4) is considered instead of (2), expression (5) remains valid for $\mu_z(\mathbf{r})$, according to the law of iterated expectations:

$$\mathcal{E}\{p_m(\mathbf{r})\} = \mathcal{E}\{\mathcal{E}\{p_m(\mathbf{r}) | E_m\}\} = \mathcal{E}\{y_m(\mathbf{r})\}.$$

As concerns the data correlation function, we have

$$\gamma_z(\mathbf{r}, \mathbf{r}') = \gamma_p(\mathbf{r}, \mathbf{r}') + \gamma_\varepsilon(\mathbf{r} - \mathbf{r}')$$

with:

$$\gamma_p(\mathbf{r}, \mathbf{r}') = \mathcal{E}\{p_m(\mathbf{r})p_m(\mathbf{r}')\} - \mathcal{E}\{p_m(\mathbf{r})\} \mathcal{E}\{p_m(\mathbf{r}')\}. \quad (23)$$

According to the law of iterated expectations,

$$\mathcal{E}\{p_m(\mathbf{r})p_m(\mathbf{r}')\} = \mathcal{E}\{\mathcal{E}\{p_m(\mathbf{r})p_m(\mathbf{r}') | E_m\}\}.$$

For $\mathbf{r}' \neq \mathbf{r}$, since $p_m(\mathbf{r})$ and $p_m(\mathbf{r}')$ are decorrelated Poisson variables given E_m , we get

$$\mathcal{E}\{p_m(\mathbf{r})p_m(\mathbf{r}')\} = \mathcal{E}\{y_m(\mathbf{r})y_m(\mathbf{r}')\}$$

while for $\mathbf{r}' = \mathbf{r}$,

$$\mathcal{E}\{|p_m(\mathbf{r})|^2\} = \mathcal{E}\{|y_m(\mathbf{r})|^2\} + \mathcal{E}\{y_m(\mathbf{r})\},$$

since a Poisson variable is of equal mean and variance. Therefore, in the case where the Poisson statistics of the data is taken into account, (7) must be replaced by

$$\gamma_z(\mathbf{r}, \mathbf{r}') = \gamma_y(\mathbf{r}, \mathbf{r}') + \mu_z(\mathbf{r})\delta_K(\mathbf{r} - \mathbf{r}') + \gamma_\varepsilon(\mathbf{r} - \mathbf{r}') \quad (24)$$

where δ_K is the Kronecker function.

APPENDIX B PROOF OF PROPERTY 5

Let q denote the impulse response of the filter defined in the Fourier domain by

$$\tilde{q}(\mathbf{u}) = \tilde{\gamma}_E^{1/2}(\mathbf{u}) \quad \text{if } \mathbf{u} \in \mathcal{D}_{\text{spec}}, \quad 0 \text{ otherwise.}$$

Akin to γ_E , q is positive semi-definite, and hence it is a Hermitian symmetric function. We have then $\tilde{\gamma}_E = \tilde{q}^2$, and hence

$$\gamma_E = q \star q. \quad (25)$$

Let us also define the following kernels:

$$f(\mathbf{r}, \mathbf{r}') = \int q(\mathbf{r} - \mathbf{x})q^*(\mathbf{r}' - \mathbf{x})\rho(\mathbf{x})d\mathbf{x}, \quad (26)$$

$$F(\mathbf{r}, \mathbf{r}') = \int f(\mathbf{r}, \mathbf{r}'')f^*(\mathbf{r}', \mathbf{r}'')d\mathbf{r}''. \quad (27)$$

and the induced integral operators K_f and K_F :

$$K_f\phi(\mathbf{r}) = \int f(\mathbf{r}, \mathbf{r}')\phi(\mathbf{r}')d\mathbf{r}',$$

$$K_F\phi(\mathbf{r}) = \int F(\mathbf{r}, \mathbf{r}')\phi(\mathbf{r}')d\mathbf{r}'.$$

According to the Cauchy-Schwartz inequality,

$$|f(\mathbf{r}, \mathbf{r}')|^2 \leq \int |q(\mathbf{r} - \mathbf{x})|^2 \rho(\mathbf{x})d\mathbf{x} \int |q(\mathbf{r}' - \mathbf{x})|^2 \rho(\mathbf{x})d\mathbf{x}.$$

As a consequence,

$$\iint |f(\mathbf{r}, \mathbf{r}')|^2 d\mathbf{r} d\mathbf{r}' \leq \left(\int |q(\mathbf{r})|^2 d\mathbf{r} \int \rho(\mathbf{x})d\mathbf{x} \right)^2,$$

where ρ is integrable, and

$$\int |q(\mathbf{r})|^2 d\mathbf{r} = \int \tilde{\gamma}_E(\mathbf{u})d\mathbf{u} = \gamma_E(0) < \infty.$$

Therefore, we have

$$\iint |f(\mathbf{r}, \mathbf{r}')|^2 d\mathbf{r} d\mathbf{r}' < \infty,$$

i.e., $f \in L^2(\mathbb{R}^d \times \mathbb{R}^d; \mathbb{C})$, and consequently, K_f is a Hilbert-Schmidt integral operator [31, Proposition 3.4.16]. On the other hand, the integral operator K_F is the square of K_f , in the sense that $K_F\phi = K_f K_f\phi$ for any ϕ . Thus, K_F is also a Hilbert-Schmidt operator.

Now let us go to the heart of the proof, which is threefold. The first step allows us to show that kernel F is uniquely defined from γ_y . In a second step, we establish that f is uniquely defined from F given (27). At this point, we conclude that the knowledge of γ_y implies that of f , which is a linear functional of ρ (whereas the dependency of γ_y in ρ is quadratic). The last step consists in a Fourier analysis of f , in order to determine which spectral components of ρ are identifiable from the knowledge of f .

Step 1) Given (26) and (25), we have the following alternate expression for (27):

$$F(\mathbf{r}, \mathbf{r}') = \iint \rho(\mathbf{x})\rho(\mathbf{x}')q(\mathbf{r} - \mathbf{x})q^*(\mathbf{r}' - \mathbf{x}')\gamma_E(\mathbf{x} - \mathbf{x}')d\mathbf{x}d\mathbf{x}'. \quad (28)$$

Comparing the latter expression to (8), it is clear that $F = \gamma_y$ in the case $q = h$, i.e., when the speckle correlation is $h \star h$. More generally, using a double Fourier transform on (28), in the same way as we obtained (10) from (8), we get

$$\begin{aligned}\tilde{F}(\mathbf{u}, \mathbf{u}') &= \tilde{q}(\mathbf{u})\tilde{q}(-\mathbf{u}')\tilde{g}(\mathbf{u}, \mathbf{u}') \\ &= \frac{\tilde{q}(\mathbf{u})\tilde{q}(-\mathbf{u}')}{\tilde{h}(\mathbf{u})\tilde{h}(-\mathbf{u}')} \tilde{\gamma}_y(\mathbf{u}, \mathbf{u}') \quad \text{if } \mathbf{u}, \mathbf{u}' \in \mathcal{D}_{\text{spec}}, \\ &= 0 \quad \text{otherwise.}\end{aligned}\quad (29)$$

Let us remark that $\tilde{h}(\mathbf{u}) \neq 0$ if $\mathbf{u} \in \mathcal{D}_{\text{spec}}$ because we have assumed $\mathcal{D}_{\text{spec}} \subseteq \mathcal{D}_{\text{PSF}}$.

Step 2) Kernel f is obviously symmetric. Moreover, it is positive semi-definite, since for any square integrable function ϕ ,

$$\iint f(\mathbf{r}, \mathbf{r}') \phi(\mathbf{r}) \phi^*(\mathbf{r}') d\mathbf{r} d\mathbf{r}' = \int |q \star \phi|^2(\mathbf{x}) \rho(\mathbf{x}) d\mathbf{x} \geq 0.$$

It is easy to check that kernel F is also positive semi-definite. Moreover K_F is bounded, since it is a Hilbert-Schmidt operator. Being bounded and positive semi-definite, K_F admits a unique square root [31, Prop. 3.2.11]. In other words, K_f is uniquely defined given K_F , and equivalently, given the kernel F , there exists a unique kernel f that fulfills (27).

Finally, the knowledge of γ_y uniquely determines F through (29)-(30), which in turn determines f .

Step 3) Eq. (26) can be written as follows in the Fourier domain:

$$\tilde{f}(\mathbf{u}, \mathbf{u}') = \tilde{q}(\mathbf{u}) \tilde{q}(-\mathbf{u}') \tilde{\rho}(\mathbf{u} + \mathbf{u}'). \quad (31)$$

The latter identity is comparable to (13) obtained in the uncorrelated speckle case. In a much similar way, we deduce that the frequency components $\tilde{\rho}(\mathbf{u})$ are identifiable from kernel f , and thus from the data correlation γ_y , for all $\mathbf{u} \in \mathcal{D}_{\text{spec}} \ominus \mathcal{D}_{\text{spec}}$.

APPENDIX C

GRADIENT OF THE KULLBACK-LEIBLER DIVERGENCE

We first note that (19) also reads

$$D(\rho) = \frac{1}{2} \log |\Gamma_z| + \frac{1}{2M} \text{Tr}(\Gamma_z^{-1} \mathbf{V} \mathbf{V}^t) + C \quad (32)$$

where C is an irrelevant constant term, and

$$\mathbf{V} = (\mathbf{v}_1 | \dots | \mathbf{v}_M) \quad \text{with} \quad \mathbf{v}_m = \mathbf{z}_m - \boldsymbol{\mu}_z. \quad (33)$$

The following identities [32, Sec.2] will be useful for the derivation of the gradient of (32):

$$\begin{aligned}\nabla_\theta \log |\mathbf{A}| &= \text{Tr}(\mathbf{A}^{-1} (\nabla_\theta \mathbf{A})) \\ \nabla_\theta (\mathbf{A}^{-1}) &= -\mathbf{A}^{-1} (\nabla_\theta \mathbf{A}) \mathbf{A}^{-1} \\ \nabla_\theta (\mathbf{A} \mathbf{B}) &= (\nabla_\theta \mathbf{A}) \mathbf{B} + \mathbf{A} (\nabla_\theta \mathbf{B}) \\ \nabla_\theta \text{Tr}(\mathbf{A}) &= \text{Tr}(\nabla_\theta \mathbf{A}) \\ \nabla_\theta (\mathbf{A}^t) &= (\nabla_\theta \mathbf{A})^t\end{aligned}\quad (34)$$

where \mathbf{A} and \mathbf{B} are two matrices that depend on a real scalar parameter θ . From these relations, we get

$$\begin{aligned}\partial_n D(\rho) &= \frac{1}{2} \text{Tr}(\Gamma_z^{-1} (\partial_n \Gamma_z)) \\ &\quad + \frac{1}{2M} \text{Tr}((\partial_n \Gamma_z^{-1}) \mathbf{V} \mathbf{V}^t + \Gamma_z^{-1} \partial_n (\mathbf{V} \mathbf{V}^t))\end{aligned}\quad (35)$$

where $\partial_n = \nabla_{\rho_n}$. The gradient of (32) is then defined by

$$\nabla D(\rho) = \mathbf{vect}\{\partial_n D(\rho)\} \quad (36)$$

where $\mathbf{vect}\{v_n\} = (v_1 | \dots | v_N)^t$. According to (35) and (34), the expressions of $\partial_n \Gamma_z$ and $\partial_n (\mathbf{V} \mathbf{V}^t)$ are required. Let \mathbf{e}_n be the n th canonical vector, \mathbf{h}_n the n th column of \mathbf{H} and $\mathbf{1} = (1 \dots 1)^t$. We get from (17)

$$\partial_n \Gamma_z = \mathbf{H} \Delta \Gamma_E \mathbf{e}_n \mathbf{h}_n^t + (\mathbf{H} \Delta \Gamma_E \mathbf{e}_n \mathbf{h}_n^t)^t \quad (37)$$

and from (33):

$$\partial_n (\mathbf{V} \mathbf{V}^t) = -E_0 (\mathbf{V} \mathbf{1} \mathbf{h}_n^t + (\mathbf{V} \mathbf{1} \mathbf{h}_n^t)^t). \quad (38)$$

The derivative of the three terms in (35) can now be obtained. On the one hand, elementary manipulations involving the trace operator allow to deduce

$$\text{Tr}(\Gamma_z^{-1} (\partial_n \Gamma_z)) = 2 \mathbf{e}_n^t \mathbf{W} \mathbf{h}_n \quad (39)$$

from (37), with $\mathbf{W} = \Gamma_E \Delta \mathbf{H}^t \Gamma_z^{-1}$. On the other hand, we have from (34) and (37):

$$\text{Tr}((\partial_n \Gamma_z^{-1}) \mathbf{V} \mathbf{V}^t) = -2 \mathbf{e}_n^t (\mathbf{W} \mathbf{V} \mathbf{V}^t \Gamma_z^{-1}) \mathbf{h}_n \quad (40)$$

and from (38):

$$\text{Tr}(\Gamma_z^{-1} \partial_n (\mathbf{V} \mathbf{V}^t)) = -2 E_0 \mathbf{h}_n^t \Gamma_z^{-1} \mathbf{V} \mathbf{1}. \quad (41)$$

According to (35) and (36), we need to vectorize the relations (39), (40) and (41) to obtain the full gradient of (32). In particular, according to the identity

$$((\mathbf{A} \text{Diag}(\rho) \mathbf{B}^t) \circ \mathbf{I}) \mathbf{1} = (\mathbf{A} \circ \mathbf{B}) \rho, \quad (42)$$

we deduce from (39) that

$$\begin{aligned}\mathbf{vect}\{\text{Tr}(\Gamma_z^{-1} (\partial_n \Gamma_z))\} &= 2 ((\mathbf{W} \mathbf{H}) \circ \mathbf{I}) \mathbf{1} \\ &= 2 ((\mathbf{H}^t \Gamma_z^{-1} \mathbf{H}) \circ \Gamma_E) \rho.\end{aligned}\quad (43)$$

Similarly, we obtain after a few manipulations

$$\frac{1}{M} \mathbf{vect}\{\text{Tr}((\partial_n \Gamma_z^{-1}) \mathbf{V} \mathbf{V}^t)\} = -\frac{2}{M} ((\boldsymbol{\Omega}^t \mathbf{V} \mathbf{V}^t \boldsymbol{\Omega}) \circ \Gamma_E) \rho \quad (44)$$

and

$$\frac{1}{M} \mathbf{vect}\{\text{Tr}(\Gamma_z^{-1} \partial_n (\mathbf{V} \mathbf{V}^t))\} = -\frac{2}{M} E_0 \boldsymbol{\Omega} \mathbf{V} \mathbf{1} \quad (45)$$

where $\boldsymbol{\Omega} = \Gamma_z^{-1} \mathbf{H}$. As a result, the gradient of (35) reads

$$\begin{aligned}\nabla D(\rho) &= \\ &\quad - \left(\left(\boldsymbol{\Omega}^t \left(\frac{1}{M} \mathbf{V} \mathbf{V}^t - \Gamma_z \right) \boldsymbol{\Omega} \right) \circ \Gamma_E \right) \rho - \frac{1}{M} E_0 \boldsymbol{\Omega} \mathbf{V} \mathbf{1}.\end{aligned}\quad (46)$$

Finally, the following relations hold:

$$\begin{aligned}\mathbf{V} &= (\mathbf{z}_1 - \hat{\boldsymbol{\mu}} | \dots | \mathbf{z}_M - \hat{\boldsymbol{\mu}}) + \boldsymbol{\delta}_\mu \mathbf{1}^t, \\ \frac{1}{M} \mathbf{V} \mathbf{V}^t &= \hat{\Gamma}_z + \boldsymbol{\delta}_\mu \boldsymbol{\delta}_\mu^t,\end{aligned}$$

which allow us to obtain the gradient expression (21), given that $\nabla J(\rho) = \nabla D(\rho) + \beta \rho$.

REFERENCES

- [1] P. Van den Berg and J. Fokkema, "Removal of undesired wavefields related to the casing of a microwave scanner", *IEEE Transactions on Microwave Theory and Techniques*, vol. 51, no. 1, pp. 187–192, 2003.
- [2] D. C. Munson, J. O'Brien, and K. W. Jenkins, "A tomographic formulation of spotlight mode synthetic aperture radar", *Proceedings of the IEEE*, vol. 71, pp. 917–925, 1983.
- [3] M. G. Gustafsson, L. Shao, P. M. Carlton, C. J. R. Wang, I. N. Golubovskaya, W. Z. Cande, D. A. Agard, and J. W. Sedat, "Three-dimensional resolution doubling in wide-field fluorescence microscopy by structured illumination", *Biophysical Journal*, vol. 94, no. 12, pp. 4957 – 4970, 2008.
- [4] O. Haeberlé, K. Belkebir, H. Giovannini, and A. Sentenac, "Tomographic diffractive microscopy: basics, techniques and perspectives", *Journal of Modern Optics*, vol. 57, no. 9, pp. 686–699, 2010.
- [5] A. J. Devaney, "A filtered backpropagation algorithm for diffraction tomography", *Ultrasonic Imaging*, vol. 4, pp. 336–350, 1982.
- [6] R. Heintzmann and C. G. Cremer, "Laterally modulated excitation microscopy: improvement of resolution by using a diffraction grating", *Proceedings of SPIE*, vol. 3568, pp. 185–196, 1999.
- [7] M. G. L. Gustafsson, D. A. Agard, and J. W. Sedat, "Doubling the lateral resolution of wide-field fluorescence microscopy using structured illumination", *Proceedings of SPIE*, vol. 3919, pp. 141–150, 2000.
- [8] P. Thibault, M. Dierolf, O. Bunk, A. Menzel, and F. Pfeiffer, "Probe retrieval in ptychographic coherent diffractive imaging", *Ultramicroscopy*, vol. 109, no. 4, pp. 338 – 343, 2009.
- [9] K. Wicker, O. Mandula, G. Best, R. Fiolka, and R. Heintzmann, "Phase optimisation for structured illumination microscopy", *Optics Express*, vol. 21, no. 2, pp. 2032–2049, Jan 2013.
- [10] R. Ayuk, H. Giovannini, A. Jost, E. Mudry, J. Girard, T. Mangeat, N. Sandeau, R. Heintzmann, K. Wicker, K. Belkebir, and A. Sentenac, "Structured illumination fluorescence microscopy with distorted excitations using a filtered blind-SIM algorithm", *Optics Letters*, vol. 38, no. 22, pp. 4723–4726, Nov 2013.
- [11] A. Jost, E. Tolstik, P. Feldmann, K. Wicker, A. Sentenac, and R. Heintzmann, "Optical sectioning and high resolution in single-slice structured illumination microscopy by thick slice Blind-SIM reconstruction", *PLoS ONE*, vol. 10, no. 7, pp. e0132174, July 2015.
- [12] J. W. Goodman, *Speckle Phenomena in Optics: Theory and Applications*, Roberts & Company, 2007.
- [13] E. Mudry, K. Belkebir, J. Girard, J. Savatier, E. Le Moal, C. Nicoletti, M. Allain, and A. Sentenac, "Structured illumination microscopy using unknown speckle patterns", *Nature Photonics*, vol. 6, no. 5, pp. 312–315, 2012.
- [14] J. Min, J. Jang, D. Keum, S.-W. Ryu, C. Choi, K.-H. Jeong, and J. C. Ye, "Fluorescent microscopy beyond diffraction limits using speckle illumination and joint support recovery", *Scientific Reports*, vol. 3, pp. No 2075, 2013.
- [15] J.-E. Oh, Y.-W. Cho, G. Scarcelli, and Y.-H. Kim, "Sub-Rayleigh imaging via speckle illumination", *Optics Letters*, vol. 38, no. 5, pp. 682–684, Mar 2013.
- [16] A. Negash, S. Labouesse, N. Sandeau, M. Allain, H. Giovannini, J. Idier, R. Heintzmann, P. C. Chaumet, K. Belkebir, and A. Sentenac, "Improving the axial and lateral resolution of three-dimensional fluorescence microscopy using random speckle illuminations", *Journal of the Optical Society of America (A)*, vol. 33, no. 6, pp. 1089–1094, June 2016.
- [17] J. Gateau, T. Chaigne, O. Katz, S. Gigan, and E. Bossi, "Improving visibility in photoacoustic imaging using dynamic speckle illumination", *Optics Letters*, vol. 38, no. 23, pp. 5188–5191, 2013.
- [18] E. Parzen, "A simple proof and some extensions of the sampling theorem", Tech. Rep. 7, Stanford University, Stanford, CA, 1956.
- [19] J. W. Goodman, *Introduction to Fourier Optics*, McGraw-Hill Physical and Quantum Electronics Series (second edition), San Francisco, 2 edition, 1996.
- [20] J. R. Lakowicz, *Principles of Fluorescence Spectroscopy*, Springer US, 3rd edition, 2006.
- [21] G. H. Golub and C. F. Van Loan, *Matrix computations*, The Johns Hopkins University Press, Baltimore, Third edition, 1996.
- [22] S. Kullback, *Information Theory and Statistics*, John Wiley, New York, NY, 1959.
- [23] M. I. Miller and D. L. Snyder, "The role of likelihood and entropy in incomplete-data problems: Applications to estimating point-process intensities and Toeplitz constrained covariances", *Proceedings of the IEEE*, vol. 75, no. 7, pp. 892–906, July 1987.
- [24] A. P. Dempster, N. M. Laird, and D. B. Rubin, "Maximum likelihood from incomplete data via the EM algorithm", *Journal of the Royal Statistical Society B*, vol. 39, pp. 1–38, 1977.
- [25] A. D. Lanterman, "Statistical radar imaging of diffuse and specular targets using an expectation-maximization algorithm", *Proceedings of SPIE*, vol. 4053, pp. 20–31, 2000.
- [26] T. Chaigne, J. Gateau, M. Allain, O. Katz, S. Gigan, A. Sentenac, and E. Bossy, "Super-resolution photoacoustic fluctuation imaging with multiple speckle illumination", *Optica*, vol. 3, no. 1, pp. 54–57, 2016.
- [27] S. Kimura and C. Munakata, "Dependence of 3-D optical transfer functions on the pinhole radius in a fluorescent confocal optical microscope", *Applied Optics*, vol. 29, no. 20, pp. 3007–3011, Jul 1990.
- [28] B. Simon, M. Debailleul, V. Georges, V. Lauer, and O. Haeberlé, "Tomographic diffractive microscopy of transparent samples", *The European Physical Journal - Applied Physics*, vol. 44, no. 1, pp. 29–35, 2008.
- [29] P. Comon and L. De Lathauwer, "Chapter 9: Algebraic identification of under-determined mixtures", in *Handbook of Blind Source Separation*, P. Comon and C. Jutten, Eds., pp. 325–365. Academic Press, Oxford, 2010.
- [30] T. Dertinger, R. Colyer, G. Iyer, S. Weiss, and J. Enderlein, "Fast, background-free, 3D super-resolution optical fluctuation imaging (SOFI)", *Proceedings of the National Academy of Sciences*, vol. 106, no. 52, pp. 22287–22292, 2009.
- [31] G. K. Pedersen, *Analysis Now*, Springer-Verlag, New York, NY, 1995.
- [32] K. B. Petersen and M. S. Pedersen, "The matrix cookbook", Tech. Rep., Technical University of Denmark, Nov. 2012.

